Simulations of Pulsed Sodium Laser Guide Stars — An Overview

Ronald Holzlöhner[1], Simon M. Rochester[2,3], Domenico Bonaccini Calia[1], Dmitry Budker[3,2], Thomas Pfrommer[1], James M. Higbie[4]

[1] TEC Optics and Photonics Department, European Southern Observatory (ESO), Karl-Schwarzschild-Str. 2, D-85748 Garching b. München, Germany, http://www.eso.org/sci/facilities/develop/lgsf/

[2] Rochester Scientific LLC, El Cerrito, CA 94530, USA

[3] University of California Berkeley, Department of Physics, Berkeley, CA 94720-7300, USA

[4] Bucknell University, Department of Physics, 701 Moore Avenue, Lewisburg, PA 17837, USA

ABSTRACT

Almost all sodium laser guide star (LGS) systems in the world are based on pulsed lasers. We review the relevant sodium physics and compare different laser pulse formats. Selected formats are discussed on the basis of numerical simulation results. One of the key findings is that the brightness of most existing LGS facilities could be boosted at, as we argue, reasonable expense. Recommendations are presented to enhance the LGS return flux and to design future LGS lasers, including those suitable for spot tracking in the mesosphere to mitigate the spot elongation problem.

Keywords: Laser guide stars, Atmospheric propagation, Laser beam transmission, Wavefront sensing

1. INTRODUCTION

Sodium laser guide stars (LGS) are used as artificial beacons for Adaptive Optics (AO) in many large telescopes. The upcoming generation of 30+m telescopes will rely for their operation on LGS-assisted AO. An LGS is a luminous column of 10–20 km height in the mesosphere, centered at about 93 km altitude, where naturally occurring sodium is excited with resonant light at 589 nm (orange), which is followed by fluorescence. The LGS facilities require lasers with excellent beam quality to minimize the spot size and a power of 5–25 watt per star. In order to optimize the brightness of the guide stars, detailed understanding of light-atom interaction physics is required. We find that the excitation efficiency depends nontrivially on the laser spectrum, polarization, the geomagnetic field, and other parameters.

While a format optimization is already a challenging task for continuous-wave (cw) lasers, any modulation of the laser power introduces an additional level of complexity to the simulation. When modeling installed systems, a good knowledge of the pulse format both in time and frequency domain is required. However, only limited data are usually available from observatories; in particular, highly resolved optical spectra and their stability in time have seldom been measured.

The return flux from sodium LGS depends on, among various other parameters, the geomagnetic field, atomic collision rates and mesospheric temperatures. Moreover, the photon return flux per atom is in general a nonlinear function of irradiance (power density) in the sodium layer.

2. MODELING SETUP

The Bloch equation system that describes sodium D_2 excitation in the mesosphere is described in detail in [1]. It can be written in matrix form as

$$\dot{\rho} = \mathbf{A}\rho + b \,, \tag{1}$$

where ρ is the density matrix expressed as a vector, containing 322 (or 576 when including more hyperfine states) states of the sodium ensemble for each velocity class, and $\mathbf{A}$ and b are a matrix and a vector, respectively, that are independent of ρ. In practice, $\mathbf{A}$ is represented as a large sparse matrix and it depends, among other parameters, on the laser irradiance, laser frequency in D_{2a} and D_{2b} and polarization incident on the atoms. In the case of cw lasers, $\mathbf{A}$ is independent of time and one simply solves the inhomogeneous linear equation system $\mathbf{A}\rho_{ss} + b = 0$ with constant coefficients, where ρ_{ss} denotes the steady state density matrix.

The Bloch matrix **A** contains many terms that depend on the incident light and hence vary in the presence of modulated lasers. However, pulses can often be approximated by a piecewise constant function, in particular during the dark periods in between pulses that are often quite long compared to the pulse duration t_p. The evolution equation within each step then again has constant coefficients and its solution is given by

$$\rho(t + \Delta t) = \exp(\Delta t\, \mathbf{A})\left(\rho(t) - \rho_{ss}\right) + \rho_{ss}, \qquad \mathbf{A}\rho_{ss} + b = 0\,, \qquad (2)$$

where the function exp() denotes the matrix exponential (which in general differs from the matrix of the exponentials of the matrix elements). Equation (2) can be efficiently solved by employing iterative sparse matrix exponential routines which are optimized and highly robust, *i.e.*, the solution does not diverge even at low accuracy settings. The first two authors of this paper have successfully employed the free package Expokit [2] which solves Eq. (2) without computing the matrix $\exp(\Delta t\, \mathbf{A})$ explicitly (we have translated the code of the Expokit subroutine `phiv` from Matlab to Mathematica, which calls the Mathematica built-in routine `MatrixExp[]` within each Krylov subspace recursion and terminates once a user-defined error tolerance threshold has been crossed). Subsequently, we have found that the single command `MatrixExp[`$\Delta t\, \mathbf{A}, \rho(t) - \rho_{ss}$`] + `$\rho_{ss}$ runs even faster. We have implemented this latter approach in the routine `StepPulseFlux[]` which has been part of the freely available *LGSBloch* simulation package [3] since 2010 and has been employed by Rampy *et al.* in [4].

For special laser formats it is possible to take advantage of certain properties of sodium physics and further speed up the solution. One example is the simulation of laser pulses whose repetition period t_{rep} is much larger than about 7τ, where $\tau = 16.25$ ns is the sodium D_2 excited state lifetime. After the excited state population has decayed to zero at $t = t_p + 7\tau$, it is sufficient to merely follow the evolution of the sodium ground states which mix due to Larmor precession and atomic collisions on the time scale of microseconds rather than nanoseconds, allowing for larger solver time steps and a much reduced number of variables. S. Rochester has recently implemented a solver based on the Sundials [5] general purpose ordinary differential equation (ODE) solver that automatically chooses between stiff and nonstiff solution algorithms and successfully applied it to the TIPC pulsed laser format, considered for TMT [6] (this accelerated solver has not been made public to date). The piecewise constant pulse profile approximation is in this case defined by the step size control of the ODE algorithm. We have validated that the Sundials based solver and the one based on matrix exponentials yield identical results for the formats in this work.

One subtlety of the numerical solution concerns the treatment of lasers with added D_{2b} repumping in which an external electro-optic phase modulator (EOM) driven at 1.710 GHz is employed (Note: The optimal repumping frequency offset of 1.710±5 GHz has been slightly revised from 1.7178 GHz in [1]), or else the seed laser in a master oscillator power amplifier (MOPA) system can be phase modulated. In our simulations we have so far assumed that the laser spectrum without the added sideband (*i.e.* when the phase modulation is turned off) only overlaps with the D_{2a} line, and conversely the blue EOM sideband only excites the D_{2b} transitions. In this case, it is possible to apply the rotating wave approximation to each transition separately, which is a precondition for **A** being constant [1]. However, when simulating wide-band pulsed or non-pulsed systems of which we give examples below, this assumption is not valid anymore since the wings of the laser line overlap with the added repumping line. If, on the other hand, no repumping modulation is added, our code automatically applies the laser power to both the D_{2a} and the D_{2b} transitions, hence we account for the entire excitation and no problem arises (we observe that the accelerated solver can take larger time steps when we neglect the D_{2b} transitions altogether, which is a good approximation for narrow-band lasers without repumping). We are planning to extend the solver so that it can correctly model very wide-band lasers with added repumping through phase modulation.

2.1 Two Key Quantities for Pulsed Lasers

We consider sodium atoms excited by periodically modulated light. In simple terms, the sodium transitions are excited at the beginning of the first light pulse on the time scale τ. Starting from sodium in thermal equilibrium, during a square pulse whose peak irradiance does not saturate, the sodium return flux grows as

$$\Psi(t) = \Psi_{ss}\left[1 - \exp(-t/\tau)\right], \qquad \Psi_{ss} = r\rho_{ss}, \qquad (3)$$

where r is the fluorescence vector needed to compute the steady-state return flux in the mesosphere Ψ_{ss} (units of ph/s/sr/atom) from the density matrix [1]. Conversely, the return flux decays exponentially with time constant τ once the pulse ends. Equation (3) implies that the flux equals a weighted sum of the excited state populations, a quantity that

depends on the excitation history of the atoms. Specifically, this excitation does not decay to zero if t_{rep} is below or comparable to τ, and hence the return flux from some quasi-cw laser formats never decays to zero.

As already mentioned, other important time scales such as the Larmor precession (period 3–6 µs, depending on the geographical location) or atomic collisions and gas diffusion (scale $\approx$ 30–100 µs) are much longer. These influence the ground state population, rendering the Bloch equations stiff and thus complicating the numerical solution.

Viewed in frequency space, roughly speaking the excited state population after a few pulses is proportional to the laser power spectrum convolved with the natural line of sodium (a Lorentzian with a full width at half maximum of $1/(2\pi\tau)$ = 9.7 MHz, giving rise to the concept of velocity classes), multiplied by the mesospheric sodium Doppler profile (Gaussian with FWHM of about 1 GHz). Since the velocity classes are decoupled over short time scales, we can effectively consider the pulse excitation in each of them independent and introduce the concept of pulse light irradiance $I_{p\tau,i}$ in velocity class i

$$I_{p\tau,i} = \frac{I_{avg}}{\varepsilon_{p\tau}} \frac{P_i}{P}, \qquad \varepsilon_{p\tau} = \min\left(\frac{t_p + \tau}{t_{rep}}, 1\right), \tag{4}$$

where I_{avg} is the mesospheric time-averaged pulse irradiance, P is the total laser power at the output of the laser launch telescope, P_i is the part of P within the velocity class i and $\varepsilon_{p\tau}$ represents a modified duty cycle in which the pulse duration is extended by τ to account for some population decay. The quantity $I_{p\tau,,i}$ can be considered the pulsed analog of the constant irradiance from a cw laser, in other words, we conceptually think of a family of cw lasers with irradiances $I_{p\tau,,i}$.

The other key quantity is the overlap of the laser spectrum with the sodium cross section, more precisely the ratio of the low-power sodium D_{2a} –D_{2b} Doppler profile, weighted by the laser power spectral density (psd), to the peak cross section σ_{max} times total laser power

$$\kappa = \int_{-\infty}^{\infty} \sigma(f)\, \text{psd}(f)\, df \bigg/ \sigma_{max} \int_{-\infty}^{\infty} \text{psd}(f)\, df, \tag{5}$$

which lies in the range between zero and one ($\kappa = 1$ corresponds to a narrow-band laser tuned to the center frequency of the D_{2a} line).

We can now roughly estimate the pulsed laser return at low laser power as

$$\Psi_{ss,\text{pulsed}} \approx \varepsilon_{p\tau} \sum_i \frac{\sigma_i}{\sigma_{max}} \Psi_{ss}\left(I_{p\tau,i}\right) \approx \varepsilon_{p\tau}\kappa \sum_i \Psi_{ss}\left(I_{p\tau,i}\right), \tag{6}$$

where $\psi_{ss}(I)$ denotes the flux from cw excitation at irradiance I and all other conditions relevant for the pulsed laser such as polarization, geomagnetic field, collision rate etc. At higher irradiance, numerous nonlinear and slow time-dependent processes set on so that Eq.(6) ceases to yield a good approximation, but the total return will still remain roughly proportional to κ (the sodium Doppler profile cannot be altered by lasers if we neglect recoil). This is why wide-band lasers suffer from a serious efficiency penalty that cannot be reversed. Furthermore, the sodium may saturate during the pulses if $I_{p\tau,i}$ significantly exceeds a value of around 200 W/m^2 (see also Fig. 3 in [1]).

Finally, we caution that the quantities $I_{p\tau,i}$ and κ are useful only in a first step of understanding pulsed LGS because all velocity classes are coupled over longer time scales, as explained before. In particular, this coupling has implications for the population migration towards the lower (F=1) ground state, known as downpumping, which can unfortunately degrade wide-band laser flux efficiency even further.

In the next section, we will use the quantity s_{ce} defined as [1] (units of ph/s/W/(atoms/m^2))

$$s_{ce} = \frac{\Phi\, X\left(H_{Na} - H_{tele}\right)^2}{P\, (T_a)^{2X}\, C_{Na}}, \tag{7}$$

where Φ is the average return flux on the ground (unit photons/s/m^2), $X \approx \sec(\zeta)$ is the airmass at zenith angle ζ, H_{Na} and H_{tele} are the sodium centroid and telescope altitudes above sea level, respectively, T_a is the one-way atmospheric transmission at zenith and at 589 nm and C_{Na} is the sodium atom column abundance. The purpose of s_{ce} is to normalize Φ by all the quantities that it depends on to first order so as to arrive at a figure of merit that characterizes the laser (pulse) format efficiency and only varies weakly with P, the geomagnetic field strength B and the angle θ between laser and

geomagnetic field lines. As an example, a circularly polarized narrow-band (< 10 MHz) cw laser tuned to the D_{2a} line center with a power fraction of $q=12\%$ in the D_{2b} line achieves $s_{ce} \approx 250$ photons/s/W/(atoms/m^2) in our simulations.

3. RESULTS AND DISCUSSION

3.1 Laser Formats

There is a wide range of pulsed LGS formats installed at observatories around the world with vastly different parameters. Table 1 shows an overview of some of the LGS lasers at large observatories and in research, both in operation and in preparation, sorted by increasing repetition rate $f_{rep} = 1/t_{rep}$. Two of the formats (Adelaide, Palomar) have a micro-macro pulse format, where a macro pulse comprises a burst of micropulses of very high peak power. Three of the lasers produce more than one laser line (LZT lidar, TIPC, Shane dye). The data originate from a questionnaire table that had been filled out by the laser responsibles/constructors and from a table maintained by CfAO [7]. We note, however, that many of the parameters are not precisely known or may have changed after hardware upgrades or realignments. In particular, short-term optical spectra with a resolution of one velocity class or below (< 10 MHz) are normally not available.

Institution / Laser	f_{rep} [Hz]	t_p [s]	Macro period / t_p	# laser lines	Actual FWHM [Hz]
LZT lidar (Hickson/Pfrommer)	50	8 n	n/a	3–4	2–3 $\times$ 460 M (?)
TIPC (considered for TMT)	800	120 µ	n/a	3	2 $\times$ 150 M (?)
Pulse tracking (ESO proposed)	5k	3µ	n/a	1	75 M
Grenoble modeless (J.-P. Pique)	10k–30k	50 n	n/a	1	2.9 G
Shane (dye laser)	11 k	150 n	n/a	1	2.2 G
LLNL (Avicola)	26 k	32 n	n/a	1	3.0 G
Keck II (dye laser)	26 k	100 n	n/a	1	2 .0 G
Univ. of Adelaide (J. Munch)	76 M	1 n	417	1	450 M
Gemini North (LMCT)	76 M	700 p	n/a	1	550 M (?)
Gemini South, Keck I (LMCT)	76 M	312 p	n/a	1	2.1 G (?)
Palomar (E. Kibblewhite)	100 M	800 p	20	1	1.6 G
Subaru (MegaOpto)	143 M	800 p	n/a	1	1.7 G

Table 1: Various pulsed LGS laser formats at large telescopes and in research. The Univ. of Adelaide laser generates macro pulses of 3 µs duration repeated at 800 Hz, the Palomar laser of 150 µs repeated at 330 Hz.

Figure 1 shows the formats listed in Table 1 distinguished by repetition rate t_{rep}, mean $I_{p\tau}$ and κ. The quantity $I_{p\tau}$ has been computed by averaging over all $I_{p\tau,i}$, weighted by the P_i and divided by P. In order to enable a fair comparison of laser formats, $I_{p\tau,i}$ has been computed for equal launched laser conditions of $P = 16$W, 0.8" seeing (500 nm at zenith) and propagation at the zenith angle $\zeta = 30°$, rather than at the laser powers that the actual systems project on the sky in reality.

Three temporal regimes can be defined, delineated by the inverse sodium lifetime $1/\tau$ and the inverse collision time, which we set to roughly $1/(100µs)$. If f_{rep} is lower than $1/(100µs)$, the sodium has enough time to completely relax to thermal equilibrium between pulses, and consequently it is sufficient to simulate a single pulse. Optical pumping can only occur within each pulse.
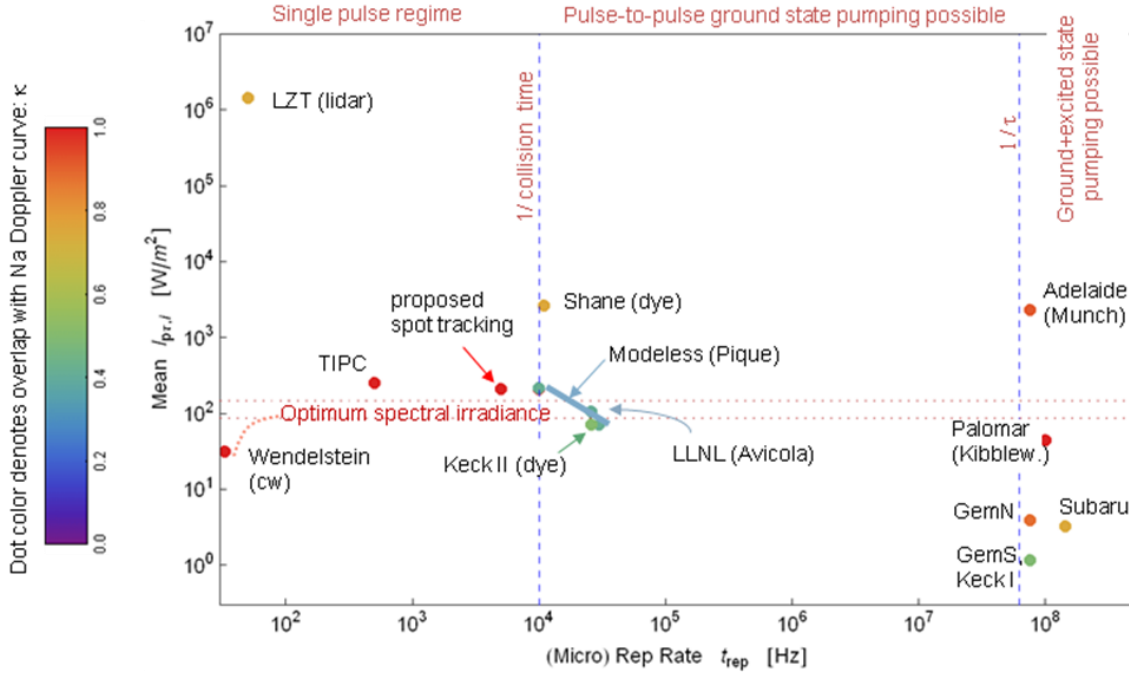
Fig. 1: The pulsed LGS formats listed in Table 1 in a plot of the mean $I_{p\tau,i}$ vs. t_{rep}

In the central regime with $1/(100\mu s) < f_{rep} < 1/\tau$, the sodium atoms can partially maintain its ground state population, in particular the ratio of atoms in $F=2$ to those in $F=1$, which equals 5/3 in thermal equilibrium. See also Rampy *et al.* find for a discussion on this point [4].

One could divide the central regime further at the inverse Larmor frequency $(1/(6\ \mu s)–1/(3\ \mu s))$: If f_{rep} exceeds this scale, it is possible to even maintain the magnetic substate and sustain optical pumping, *e.g.* into the excited states $(F=2, m=\pm 3)$ when using circular polarization. Finally, if $f_{rep} > 1/\tau$, some fraction of the excited state population will persist from pulse to pulse.

The optimal value of mean $I_{p\tau}$ is shown by the two red dashed lines for two different values of the geomagnetic field, see p.13 in [1].

The spectral overlap κ is indicated by the dot color, where reddish hues are optimal. In order to achieve good efficiency, a dot should hence lie close to the red dashed lines and be red; this is only the case for the TIPC pulse format [6], the Palomar laser and the proposed spot tracking format. For comparison, we have added a dot for the Wendelstein cw format on the left edge of the plot.

The formats pertaining to the dots far above the red dotted lines will saturate the sodium layer (stimulated emission), which generally is more detrimental than if the irradiance is low. This affects in particular the Shane, Adelaide, and LZT lidar formats (the latter is optimized for short pulses to achieve good spatial lidar resolution and observed by a 6-meter telescope so that low efficiency is not a problem).

It is interesting to note that the existing LGS lasers essentially fall into one of two categories: $f_{rep} \approx 1/$collision time, or else $f_{rep} \approx 1/\tau$. All of the more recently built lasers (Palomar, Gemini North and South, Subaru) lie in the latter group, and most of them suffer from suboptimal κ.

In the following, we discuss three different formats in greater detail: Gemini South (LMCT), Univ. of Adelaide (J. Munch) and we study a proposed long-pulse pulse format for spot tracking.

3.2 The Gemini South / Keck I Laser Format

The Gemini South and Keck I lasers have been built by Lockheed Martin Coherent Technologies and based on sum-frequency generation of 1064 nm and 1319 nm mode-locked pulse trains [8]. It is the successor of the earlier Gemini North pulse format with a pulse duration of 700 ps, but with a reduced pulse duration of 312 ps [9]. The repetition rate is 77 MHz, corresponding to t_{rep} = 13 ns which is smaller than the sodium lifetime, thus ε_{pr} = 1 according to Eq.(4). Gaussian pulses of 312 ps FWHM duration correspond to a transform-limited full width of $2\ln2/\pi$ / 312×10^{-12} s = 1.41 GHz, however, the measured bandwidth lies reportedly at about 2.1 GHz [10], which means that the pulses are shaped strongly non-Gausssian and/or there must be significant phase modulation.

A risk with wide-band lasers is that the laser itself enhances downpumping of the sodium atoms, *i.e.*, the atoms in a velocity class excited by a portion of the laser spectrum at the cycling transition $F=2\leftrightarrow F=3$ can also be excited to a state in the $F=2$ group by a spectral component 60 MHz below the $F=2\leftrightarrow F=3$ transition and moreover to the $F=1$ group by a spectral component 34 MHz further below [11]. Once the atom is in one of those excited state groups, it can decay towards the $F=1$ lower ground state and thus can only be reexcited with light at the D_{2b} transition frequency. The repetition frequency of the LMCT guide star lasers has been chosen to equal 60+34/2 = 77 MHz, the center between these two downpumping paths, presumably in order to inhibit downpumping as much as possible.

If there was zero phase noise in the laser light, the spectrum would be a perfect comb spaced by f_{rep}, *i.e.*, there would be no power across about six velocity classes between two spectral lines. In reality, however, phase noise tends to fill those spectral gaps, and furthermore the excited velocity classes are broadened by recoil, so that the LMCT laser format likely induces some accelerated downpumping.

Figure 2 displays some simulation results for the Gemini South/Keck I format. The simulation parameters are as follows, see [1] for complete definitions: Launched power: $P = 0...20$ W, linear polarization, $q = 0$ (*i.e.*, no repumping through phase modulation), t_{rep} = 13 ns, t_p = 300 ps, Gaussian pulses approximated by 15 steps, $\theta = 90°$ (angle between laser and field lines), $B = 0.23$ G (geomagnetic field strength in northern Chile), $T_a = 0.84$ (one-way atmospheric transmission), $\zeta = 30°$ (zenith angle).

Plot 2*a*) presents the time-extrapolated return flux Ψ for five differences values of I_{avg} along with the three-parameter fit function (blue curve) $\Psi(I_{avg}) = \Psi_0 \ln(1 + (I_{avg}/I_0)^c)$. Plot 2*b*) shows the evolution of the normalized flux $\psi(t) = \Psi(t)/I_{avg}$ during the first 20 periods of the simulation. Due to the normalization, the five simulation traces almost overlap in this plot. As mentioned earlier, the excited state population seemingly approaches a steady state after about 7τ. However, Plot 2*c*) indicates that there is a significant decay of $\psi(t)$ over more than 100 μs. The simulation comprises 7,700 pulse periods and consumed 21 days on a dedicated Xeon 2.5 GHz 4-core Intel Linux server and about 250 MB of RAM per simulation point, which run in parallel. Plot 2*d*) is an extrapolation to 15,000 periods or about 200 μs with the three-parameter fit function $\psi(t) = a + b \exp(-t/t_0)$ (dots: simulation samples, solid curves: extrapolation). The fit values of a are considered an approximation of $\psi(t\rightarrow\infty)$ and indicated by the dots in Plot 2*a*).

Figure 3 provides some insight to the cause of the slow decay of $\psi(t)$. The left column shows plots of the ground state population evolution of the three $F=1$ (dashed curves) and five $F=2$ (solid curves) states along the simulation in the velocity class at the D_{2a} line center for values of I_{avg} indicated by the red dot (2.38 W/m^2), pink dot (52.2 W/m^2), and cyan dot (100 W/m^2) in Fig. 2*a*. Some of the curves overlap due to symmetry and all start at 0.125 = 1/(3+5), the thermal equilibrium value (the relative energy difference between $F=1$ and $F=2$ is negligible). The yellow curve pertains to an $F=2$ state, although its line appears somewhat broken in the plots. Strong downpumping is evident (note that the left column plots only show the ground state populations in the central and thus most strongly excited velocity class; the downpumping at other spectral peaks may be less pronounced).

The plots in the right column show the excited state population for each simulated spectral bin (equals roughly one velocity class each) versus the frequency offset relative to the D_{2a} line center and scaled by the number of velocity classes (positive frequency offset moves towards the blue). The unevenness of the comb envelope is partly caused by the variable ratio of the repetition rate to the widths of the spectral bins in the simulation (which are adaptively chosen), and hence largely due to a sampling artifact that does not impact the accuracy of the numerical result. However, the spectral lines of the laser are clearly visible, along with a recoil "shoulder" each.

In order to mitigate the downpumping, we recommend applying D_{2b} repumping by adding phase modulation at 1.710 GHz to the laser and carefully adjusting the launched polarization state to circular. There are affordable external
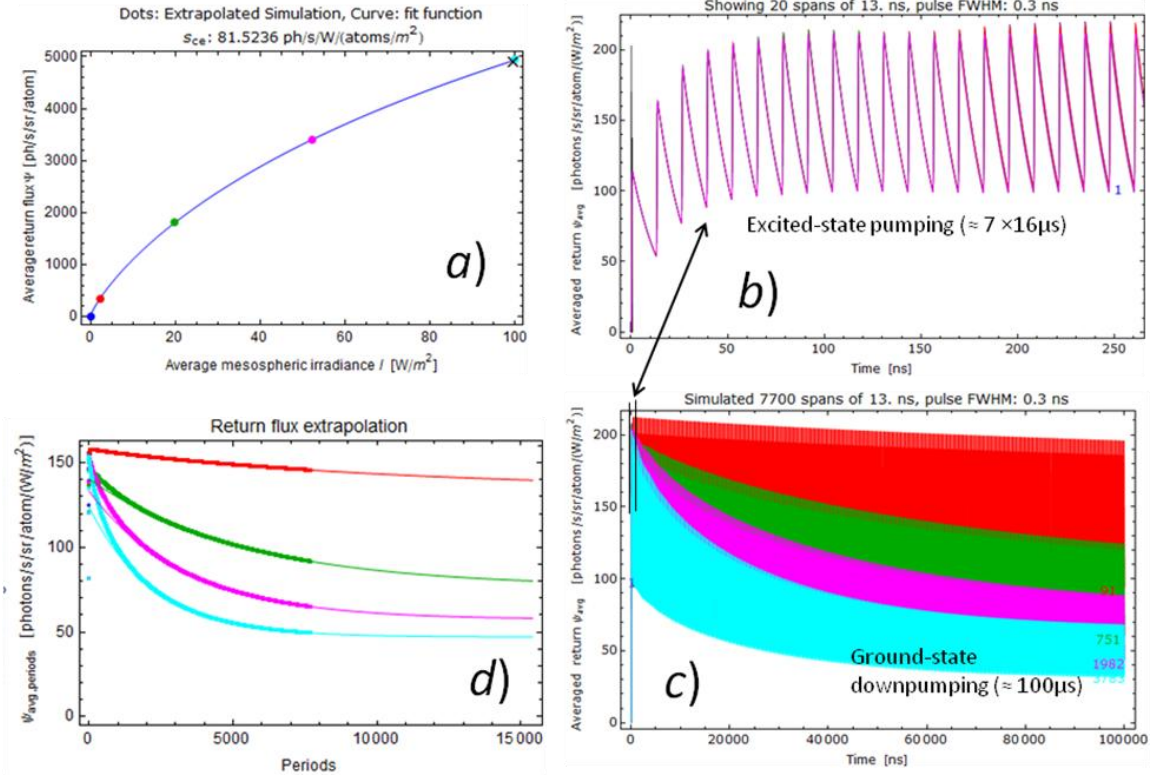
Fig. 2: Simulation of the Gemini South/Keck I laser format (LMCT). *a*) Average absolute return flux $\Psi_{ss}(I_{avg})$ of five different irradiance levels with interpolating curve (same colors used throughout), *b*) $\psi = \Psi(I_{avg})/I_{avg}$ over first 20 pulse periods (five curves with strong overlap); *c*) The full simulation time span of 100 μs (7,700 periods); *d*) Extrapolation to 15,000 periods (200 μs)

bulk optics EOMs available from manufacturers such as New Focus or Qubig [12]. If phase modulation is not an option, the efficiency of short-pulsed wide-band lasers may be somewhat boosted by aligning the frequency comb with the D_{2a}–D_{2b} frequency offset, specifically setting $f_{rep} = 1710 \pm 5$ MHz / 22 = 77.73±0.23 MHz (currently, $f_{rep} = 76.8$ MHz at Gemini South, implying a mismatch of 1710 MHz − 22×76.8 MHz = 20.4 MHz, equaling about two velocity classes). This way, at least the spectral lines in the red side of the laser spectrum each have a sibling at 1.71 GHz towards the blue so that they are repumped.

Unfortunately, it is currently not possible to model the exact effect of phase modulation repumping due to a limitation of the simulation code for very wide-band lasers, and in lieu of a measured optical laser spectrum.

All results presented so far are for single values of the mesospheric irradiance. In order to obtain the total flux from a laser spot with a nonconstant profile, we need to integrate across the irradiance distribution [13]. Figure 4 shows in Plot 4*a*) the total return flux on the ground Φ (unit photons/s/m^2) and in Plot 4*b*) the LGS laser figure of merit s_{ce}, both as a function of launched laser power. Furthermore, Plot 4*c*) displays the second moment of the return spot size which exceeds the uplink laser FWHM spot size of 0.396 m due to the nonlinearity of $\Psi(I_{avg})$. If there was no turbulence on the downlink, this plot would yield the observed spot size. Plot 4*d*) shows a table from Neichel *et al.* [9] which lists a measured flux of 10.7–17.0 ph/cm^2/s/W, corresponding to 0.4–0.7×10^6 ph/s/m^2 on the ground at GemS, while Plot 4*a*) shows an expected value of $\Phi = 1.5 \times 10^6$ ph/s/m^2, *i.e.*, a factor 2–3 more ($s_{ce} = 125$ ph/s/W/(atoms/m^2) at $P = 4$ W, but only $s_{ce} = 80$ ph/s/W/(atoms/m^2) at $P = 20$ W). However, the present simulation assumes transform-limited pulses and thus no phase noise, implying a laser bandwidth of 1.41 GHz, while in reality, as stated a bandwidth closer to 2.1 GHz has been measured.
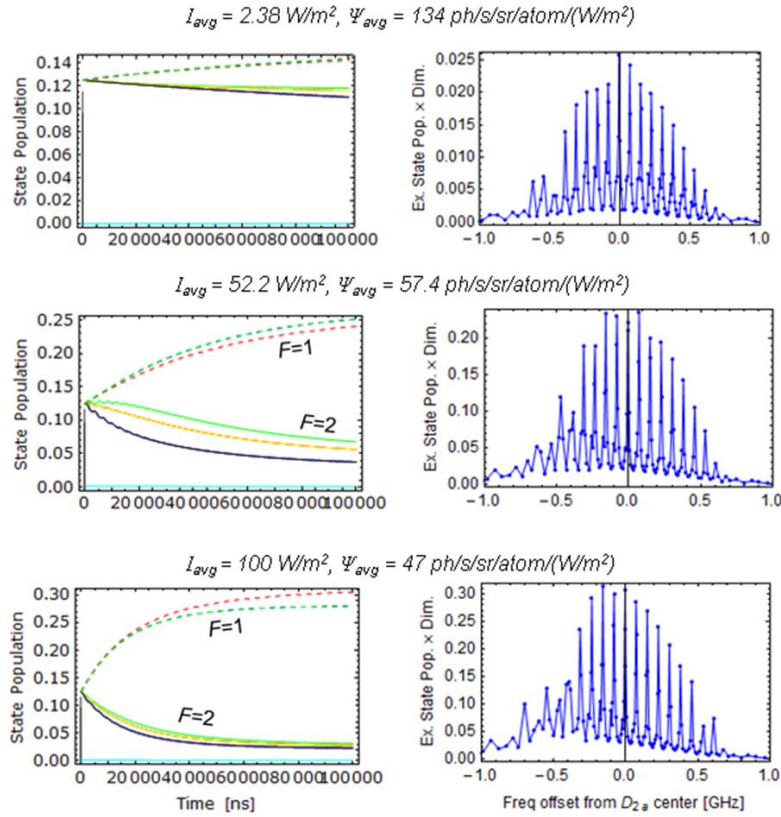
Fig. 3: Gemini South/Keck I: Left column: Ground state population evolution of the three $F=1$ (dashed) and five $F=2$ (solid curves) states at the D_{2a} line center for the values of I_{avg} indicated by the red, pink, and cyan dots in Fig. 2a. Right column: Total excited state populations across the velocity class spectrum, multiplied by the number of velocity classes.
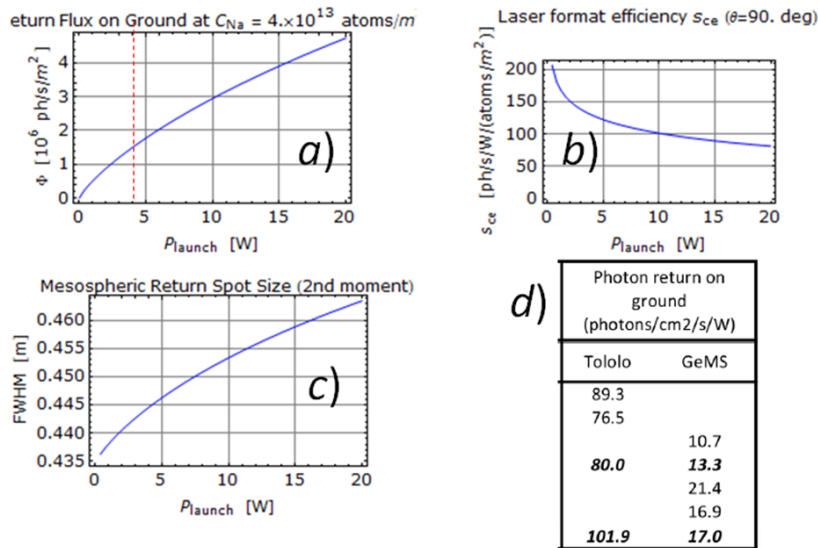
Fig. 4: Gemini South/Keck I: a) Total flux on the ground Φ (unit photons/s/m^2) versus launched laser power (red dashed line: Gemini South power level of 4 W) ; b) Merit parameter s_{ce}; c) Mesospheric FWHM return spot size; d) Measured return flux at Gemini South in photons/cm^2/s/W (courtesy B. Neichel [9])

We have repeated the described simulation but set the polarization state to circular. In this case, the simulated flux on the ground rises slightly to $\Phi = 1.75 \times 10^6$ ph/s/m^2. When repumping is added, the polarization state will make a larger difference.

3.3 The University of Adelaide Format

We now apply the same analysis to the University of Adelaide research laser pulse format [14]. Figure 5 is similar to Fig. 2. This format consists of macropulses of 3 μs duration repeated at 800 Hz that in turn contain about 230 micropulses of 1 ns FWHM duration repeated at 76 MHz.

Figure 5 shows a simulation of the first 100 micropulses within a macropulse (same simulation parameters as for Gemini South, but circular polarization). The time averaging of the shown irradiance values ignores the macropulsing, *i.e.*, one would have to multiply by the macro duty cycle of $\varepsilon_{macro} = 3$ μs $\times$ 800 Hz $= 0.24\%$ to obtain the global time average (because of the short micro repetition time of $t_{rep} = 1/76$ MHz $< \tau$, we obtain $\varepsilon_{macro} = \varepsilon_{p\tau}$ in this format). Due to the macropulsing, the peak irradiances are enhanced by the factor 0.3 ns/1 ns/$\varepsilon_{macro} = 125$ compared to the Gemini South format, which induces spontaneous emission as demonstrated by Plot 5*b*) and 5*d*): As I_{avg} rises (follow the curves from top to bottom), the normalized return $\psi(I_{avg}, t)$ not only diminishes overall, but also already decays during the laser pulse ("return narrowing"). Plot 5*a*) shows a roll-over of the absolute return $\Psi_{ss}(I_{avg})$, also indicating strong saturation. The efficiency is very low with $s_{ce} = 43$ ph/s/W/(atoms/m^2) at $P = 20$W.

Figure 6 shows analogously to Fig. 3 the ground and excited state populations (the total excited state population is shown in cyan in the left column plots). The laser spectral comb only has a FWHM width of $2\ln2/\pi / 1.0 \times 10^{-9}$ s $= 441$ MHz and the spacing of the peaks is identical to the Gemini South/Keck I format, but in the present case, one observes spectral broadening which fills the spectral gaps. Interestingly, downpumping is not a major problem of this format (also because the macropulses are much shorter than 100 μs) and circular polarization even enables optical pumping to ($F=2$, $m=2$).
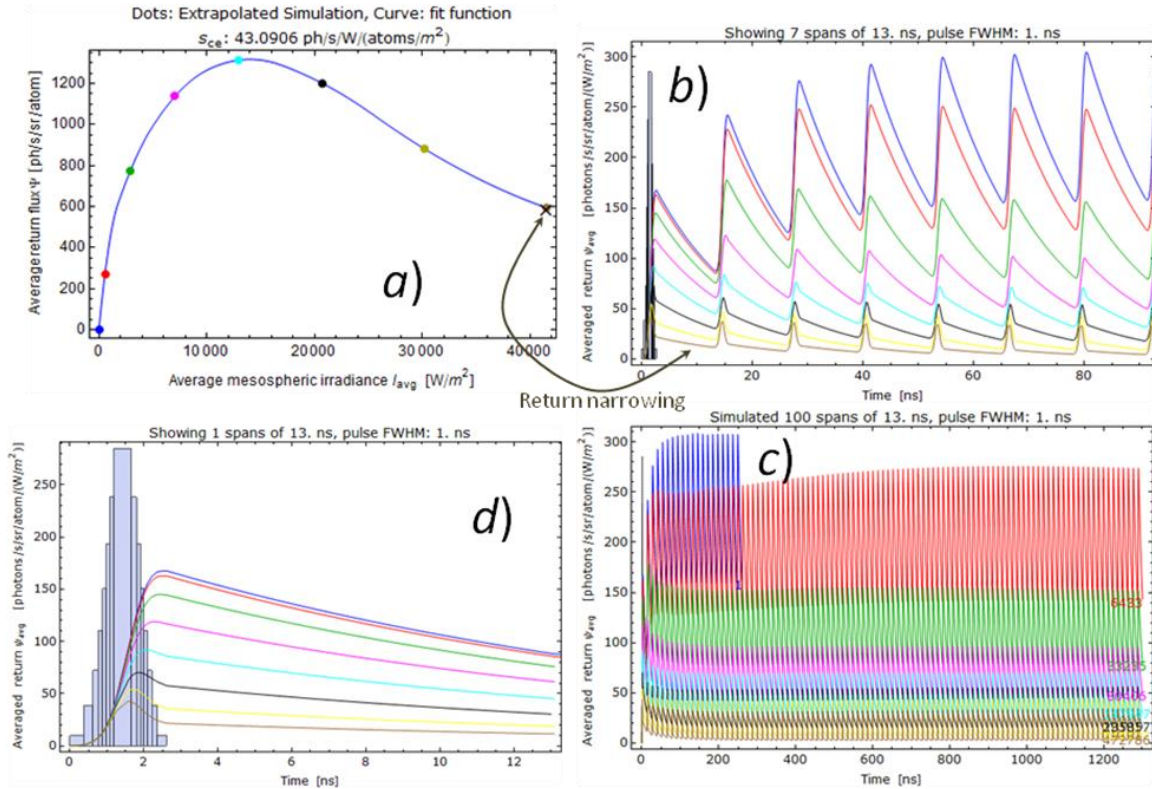
Fig. 5: Univ. of Adelaide (J. Munch). *a*) Average absolute return flux $\Psi_{ss}(I_{avg})$ at eight different irradiance levels with interpolating spline curve (same colors used throughout), *b*) Normalized flux $\psi(I_{avg}, t)$ over the first seven pulse periods (first Gaussian pulse overlaid); *c*) The full simulation time span of 1.3 μs (100 periods); *d*) Zoom into the first pulse period
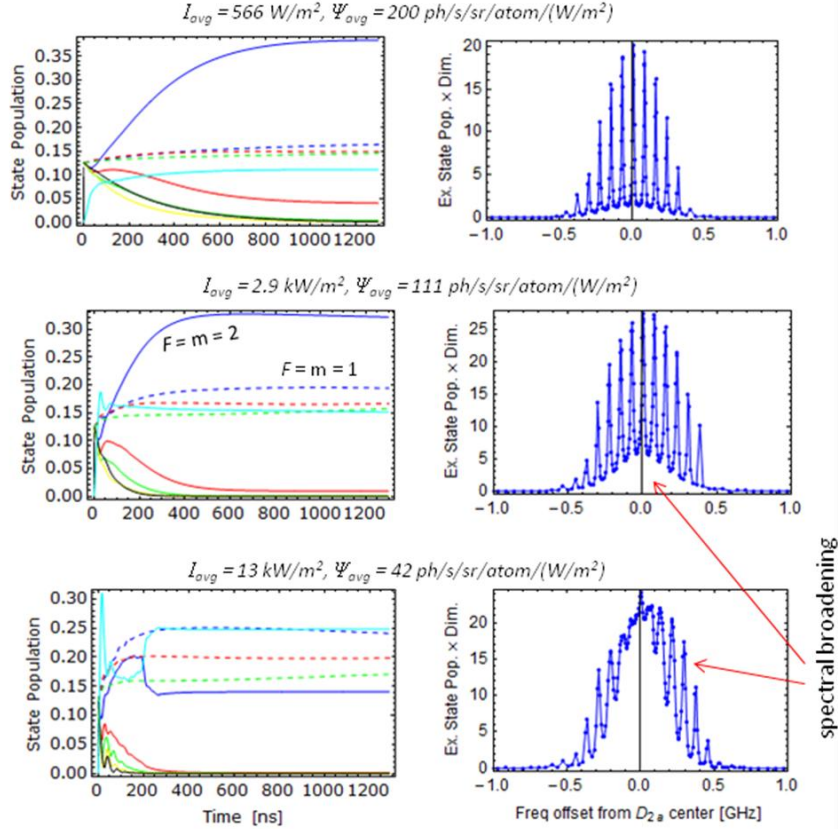
Fig. 6: Univ. of Adelaide (J. Munch): Left column: Ground state population evolution of the three $F=1$ (dashed) and five $F=2$ (solid curves) states at the D_{2a} line center for the values of I_{avg} indicated by the red, green, and cyan dots in Fig. 5a. Right column: Total excited state populations across the velocity class spectrum, multiplied by the number of velocity classes.

3.4 ESO Proposed Pulse Tracking Format

Finally, we study a pulse format that we have proposed in [13] suitable for pulse tracking to mitigate spot elongation in EELTs. It consists of square pulses of $t_p = 1\text{–}3$ μs duration, repeated at a rate of 5–10 kHz, implying $\varepsilon_{p\tau} = 0.5\ldots3\%$. We use circular polarization and D_{2b} repumping through phase modulation with a power fraction of $q = 0.12$ and an intrinsic FWHM laser linewidth of 50 MHz in order to keep $I_{p\tau,,i}$ below 200 W/m^2. Due to the rather large pulse duration, this format could be realized as a chopped cw laser with a (peak) power of about 400 W.

Figure 7 shows the return flux analogously to Figs. 2 and 5. Plot 7a) displays a rather straight curve of $\Psi(I_{avg})$, indicating a low degree of saturation. Plot 7b) indicates optical pumping during a pulse, with the return curves at several irradiance levels rising. According to Fig. 1, the rep rate is low enough for inter-pulse effects to die away, and thus it is sufficient to simulate a single pulse.

Figure 8, analogous to Figs. 3 and 6, suggests that there is still some depletion of the $F = 2$ ground state during each pulse, competing with the optical pumping. The slight kinks in the population curves near $t = 1200$ ns and 500 ns in the left plots in the second and third rows, respectively, are due to the adaptive repartitioning of the plotted spectral bins and hence do not indicate a sudden physical change in the occupation. At high irradiance, the ($F=2$, $m=2$, solid blue curve) state is pumped by the circularly polarized light with repumping and keeps growing, always competing with the unwanted ($F=1$, $m=2$, dashed blue curve) state.

The efficiency of this format at $s_{ce} = 245$ ph/s/W/(atoms/m^2) is close to that of a 20 W cw laser and thus much higher than that of short-pulse formats.
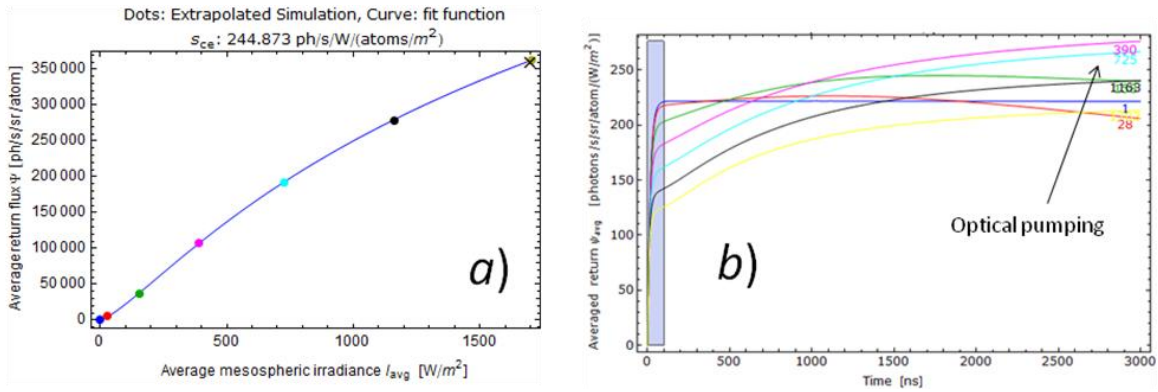
Fig. 7: ESO proposed pulse tracking format: *a*) Average absolute return flux $\Psi(I_{avg})$ of seven different irradiance levels with interpolating spline curve (same colors used throughout); *b*) Return flux evolution of $\psi(I_{avg}, t)$ during a 3 µs pulse, labeled by I_{avg}
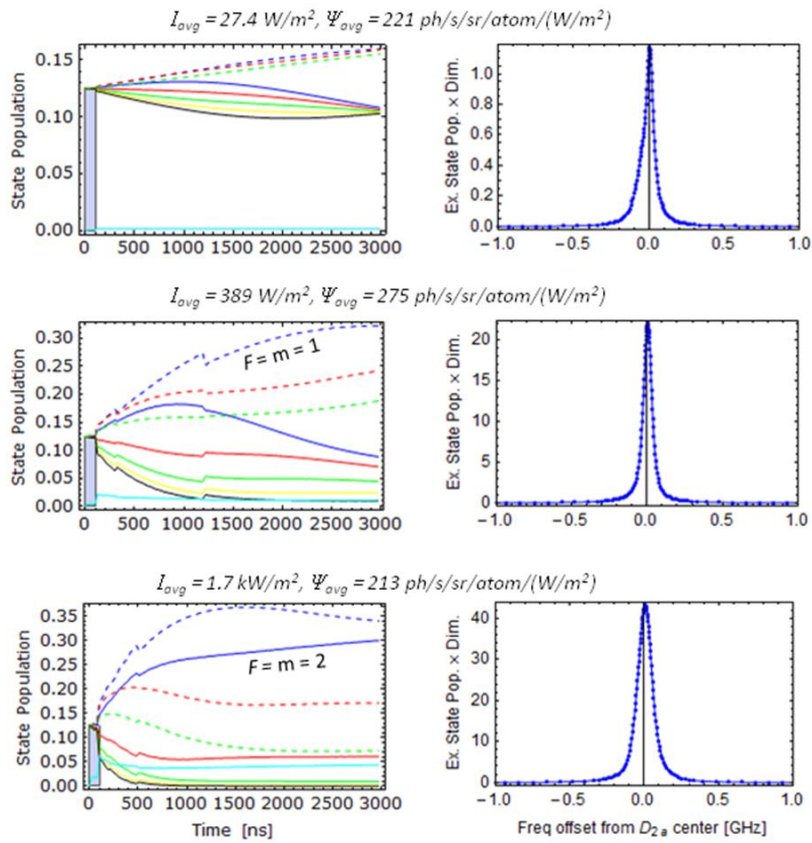
Fig. 8: ESO proposed pulse tracking format: Ground state population evolution of the three $F=1$ (dashed) and five $F=2$ (solid curves) states at the D_{2a} line center for the values of I_{avg} indicated by the red, pink, and light green dots in Fig. 7a. Right column: Total excited state populations across the velocity class spectrum, multiplied by the number of velocity classes.

4. SUMMARY AND CONCLUSIONS

Sodium laser guide stars must not only be bright, but achieve a high efficiency in terms of time-averaged return flux per watt of launched laser power. Almost all LGS lasers at large telescopes around the world are pulsed. We introduce two scalar quantities, namely spectral overlap with the sodium D_{2a}–D_{2b} profile (κ) and peak pulse irradiance per velocity class ($I_{p\tau,i}$) to characterize them.

We present an overview of the parameter range and study two short-pulse formats in detail (Gemini South/Keck I and a research format by the University of Adelaide). Finally, we evaluate a proposed long-pulse format suitable for spot tracking to mitigate spot elongation in ELTs.

The efficiency of short-pulse formats without repumping is low and suffers from low κ and strong downpumping to the lower sodium ground state (F=1) due to the wide spectrum. We propose to boost their efficiency by adding an external D_{2b} phase modulator at 1710±5 MHz to enable repumping. The launched polarization state should be circular. As a quick measure before adding a phase modulator, one may adjust the repetition rate to 1710 MHz / 22 = 77.7±0.2 MHz so that the spectral comb can repump its red wing. A detailed study of repumping gains in short-pulse lasers remains to be done. Additional macro-pulsing, while maintaining the average laser power, induces stimulated emission and thus causes a further efficiency penalty.

If pulsed LGS systems are to be deployed in the future, we recommend that a numerical analysis be carried out early in the design phase. In general, long pulses (> 100 ns) and moderate duty cycles are advisable in order to both maximize κ and to limit $I_{p\tau,i}$. However, we cannot give a simple formula to estimate the efficiency of arbitrary pulsed laser formats at higher powers due to the complexity of sodium physics.

We find that the efficiency of the proposed spot tracking format with repumping (3 µs pulses, average power about 10 W, peak power 400 W) approaches that of a 20 W narrow-band cw laser, provided that the bandwidth is raised to about 50 MHz.

REFERENCES

[1] Holzlöhner, R., Rochester, S. M., Bonaccini Calia, D., Budker, D., Higbie, J. M. and Hackenberg, W., "Optimization of cw sodium laser guide star efficiency," Astron. & Astrophys. **510**, A20 (2010)

[2] Expokit package available at http://www.maths.uq.edu.au/expokit/

[3] AtomicDensityMatrix and LGSBloch packages available at http://budker.berkeley.edu/ADM/

[4] Rampy, R., Gavel, D., Rochester, S., and Holzlöhner, R., "Investigations of Long Pulse Sodium Laser Guide Stars", Proc. SPIE 8447-170 (2012)

[5] Sundials ODE solver available at http://computation.llnl.gov/casc/sundials/

[6] Rochester, S.M., Otarola, A., Boyer, C. *et al.*, "Modeling of Pulsed Laser Guide Stars for the Thirty Meter Telescope Project", to be submitted to J. Opt. Soc. Am. B, preprint available at http://arxiv.org/abs/1203.5900

[7] CfAO LGS laser comparison table at http://lao.ucolick.org/static/SodiumLaserGuidestars_Frameset.html

[8] Lee, I., Jalali, M., Vanasse, N., *et al.*, "20 W and 50 W guidestar laser system update for the Keck I and Gemini South telescopes," Proc. SPIE 7015, 70150N (2008); http://dx.doi.org/10.1117/12.790534

[9] Neichel, B., Callingham, J., d'Orgeville, C., et al., "Characterization of the Sodium Layer at Cerro Pachon, and Impact on GemS Performance," Proc. SPIE 8447-176 (2012)

[10] d'Orgeville, C., private communication (2012)

[11] Steck, D.A., "Sodium D Line Data," rev.2.1.4 (2010), available at http://steck.us/alkalidata/sodiumnumbers.pdf

[12] Qubig GmbH, http://www.qubig.de/

[13] Holzlöhner, R., Rochester, S.M., Pfrommer, T., *et al.*, "Laser guide star return flux simulations based on observed sodium density profiles," Proc. SPIE 7736, p. 77360V (2010)

[14] Rutten, T. P., Veitch, P. J. and Munch, J., "Development of a Sodium Laser Guide Star for Astronomical Adaptive Optics Systems," Proc. *CLEO*, paper JWA92 (2007) http://www.opticsinfobase.org/abstract.cfm?URI=QELS-2007-JWA92